Geometrically incompatible confinement of solids

Benny Davidovitch[a,1], Yiwei Sun[a], and Gregory M. Grason[b,1]

[a]Department of Physics, University of Massachusetts, Amherst, MA 01003; and [b]Department of Polymer Science and Engineering, University of Massachusetts, Amherst, MA 01003

Edited by Tom C. Lubensky, University of Pennsylvania, Philadelphia, PA, and approved November 26, 2018 (received for review September 10, 2018)

The complex morphologies exhibited by spatially confined thin objects have long challenged human efforts to understand and manipulate them, from the representation of patterns in draped fabric in Renaissance art to current-day efforts to engineer flexible sensors that conform to the human body. We introduce a theoretical principle, broadly generalizing Euler's *elastica*—a core concept of continuum mechanics that invokes the energetic preference of bending over straining a thin solid object and that has been widely applied to classical and modern studies of beams and rods. We define a class of geometrically incompatible confinement problems, whereby the topography imposed on a thin solid body is incompatible with its intrinsic ("target") metric and, as a consequence of Gauss' *Theorema Egregium*, induces strain. By focusing on a prototypical example of a sheet attached to a spherical substrate, numerical simulations and analytical study demonstrate that the mechanics is governed by a principle, which we call the "Gauss–Euler *elastica*." This emergent rule states that—despite the unavoidable strain in such an incompatible confinement—the ratio between the energies stored in straining and bending the solid may be arbitrarily small. The Gauss–Euler *elastica* underlies a theoretical framework that greatly simplifies the daunting task of solving the highly nonlinear equations that describe thin solids at mechanical equilibrium. This development thus opens possibilities for attacking a broad class of phenomena governed by the coupling of geometry and mechanics.

elasticity | pattern formation | variational calculus | wrinkles

The spatial confinement of thin, solid objects has been the target of theoretical inquiry since the very early formulations of continuum mechanics. The best-known example is "Galileo's beam," a problem that is central to solid mechanics and, moreover, to the foundations of variational calculus. Considering the buckling of a wooden beam, Euler recognized that the problem is described by the variational principle (1),

$$\text{Euler's } \textit{elastica}: \quad \delta U_{\text{bend}} = 0; \text{ subject to } U_{\text{strain}} = 0\,, \qquad [1]$$

where U_{bend} and U_{strain}, respectively, are the contributions to the elastic energy of a solid rod due to bending and straining, and δU represents the first variation of U with respect to shape. Eq. **1**, known as "Euler's *elastica*," is borne out of two principles that interweave mechanics and geometry. First, thin solids are energetically far less costly to bend than to stretch, owing to the fact that the ratio of bending to stretching moduli for a rod (or sheet) of thickness t varies as $\sim t^2$ (2). Second, confining a rod in space—say, by forcing its ends to be closer than its contour length—can generically be done without straining its centerline. Thus, by restricting configurations to isometric deformations (i.e., $U_{\text{strain}} = 0$), one guarantees that they acquire minimal energy as $t \to 0$, thereby greatly reducing the space of possible equilibria states, making the problem analytically tractable.

Euler's rule can be extended to 2D solids under particular circumstances in which the deformed midsurface can be embedded in 3D isometrically (i.e., without strain) (3), for example, when analyzing the "developable cones" realized by gently pushing a Xerox paper into a ring (4). However, when addressing the generic problem of confinement of a thin solid in 3D space—namely, confinements that require a change in Gaussian curvature of the midsurface—Gauss' *Theorema Egregium* implies that a perfectly isometric deformation of the midsurface is impossible (5), revoking the applicability of Euler's variational rule (1) and requiring, instead, minimization of the fully fledged Föppl–von Kármán (FvK) energy (2),

$$\text{FvK}: \quad \delta[U_{\text{bend}} + U_{\text{strain}}] = 0\,. \qquad [2]$$

The unavoidable strain inherent to such geometrically incompatible confinement (GIC) underlies both the impossibility of drawing an accurate map of the globe as well as the frustration of gift-wrapping a ball. A quintessential example of GIC is given by the "spherical stamping" experiments of Hure et al. (Fig. 1*A*), in which a thin sheet (of size W and thickness t) is placed in a narrow gap (2δ) between two rigid, concentric spherical shells (of radius R) (6). Here, the positive Gaussian curvature of the confining topography gives rise to complex patterns that cannot be described by Euler's variational rule, necessitating consideration of the highly nonlinear interplay between bending and strain in the FvK equations.

In this work, we aim to bridge the gap between the bending-dominated mechanics of Euler and strain-dominated geometry of Gauss through the "Gauss–Euler *elastica*"—a proposed principle that generalizes the variational rule (1) and characterizes the mechanical equilibrium of GIC problems. We define GIC as the imposition of a smooth "substrate," whose shape has a Gaussian curvature, $G_{\text{sub}}(\mathbf{x})$, onto a thin solid sheet or shell, whose "target" metric is characterized by a different curvature, $G_{\text{tar}}(\mathbf{x})$. In addition to $G_{\text{sub}} - G_{\text{tar}} \neq 0$, a GIC problem is equipped with two dimensionless parameters, denoted χ^{-1} and ϵ^{-1}, which characterize, respectively, the confinement strength and the bendability of the confined solid. In what follows, we will show how to define these parameters for other GIC problems (e.g., Fig. 1 *B–F*), but to begin, their meaning is best understood through the spherical stamping problem, where

Significance

The complex morphologies of confined skins (e.g., a candy wrapper or a wrinkled elbow) emerge from the generic conflict between their susceptibility to buckling even under minute compression and the unavoidable strain in conforming geometries. Our study of the implications of this conflict leads to the formulation of an effective principle—the Gauss–Euler *elastica*—that characterizes the feasible deformations of thin sheets subject to "geometrically incompatible confinement."

Author contributions: B.D. and G.M.G. designed research; B.D., Y.S., and G.M.G. performed research; and B.D. and G.M.G. wrote the paper.

The authors declare no conflicts of interest.

This article is a PNAS Direct Submission.

[1]To whom correspondence may be addressed. Email: bdavidov@physics.umass.edu or grason@mail.pse.umass.edu.

This article contains supporting information online at www.pnas.org/lookup/suppl/doi:10.1073/pnas.1815507116/-/DCSupplemental.

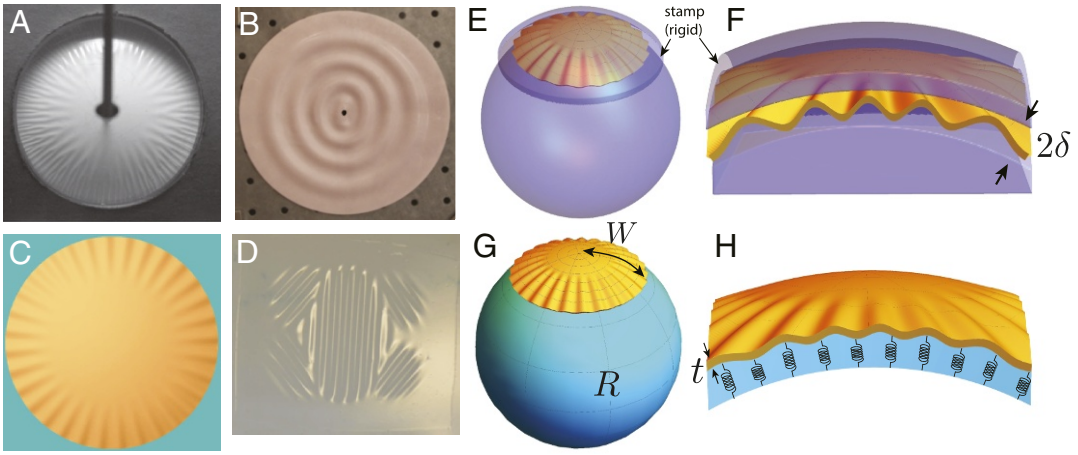

Fig. 1. (*A–D*) Examples of GIC of thin sheets/shells. (*A*) Circular sheet in a spherical stamp. Reprinted with permission from ref. 6. Copyright 2012 by the American Physical Society. (*B*) Top view of conical sheet confined between rigid, planar plates. Image courtesy of Eran Sharon (The Hebrew University of Jerusalem, Jerusalem). (*C*) Top view of simulated flat sheet confined to a "spherical Winkler" substrate (schematically drawn in *G* and *H*). (*D*) A polygonal patch cut from a thin spherical shell floated at a (planar) air/liquid interface. Image courtesy of O. Albarrán (Max Planck Institute for Dynamics and Self-Organization, Göttingen, Germany), D. V. Todorova (University of Pennsylvania, Philadelphia), E. Katifori (University of Pennsylvania, Philadelphia), and L. Goehring (Nottingham Trent University, Nottingham, United Kingdom). (*E* and *F*) A schematic of the system shown in *A*. (*G* and *H*) A schematic of the spherical Winkler model in *C*. A thin sheet is attached to a sphere made of $N \gg 1$ radial harmonic springs, with rest length R and spring constant $4\pi R^2 K_{\rm sub}/N$.

$G_{\rm sub} = R^{-2} > G_{\rm tar} = 0$. Considering $t \ll \delta \ll W \ll R$, the confinement strength and bendability are conveniently defined as:

$$\chi^{-1} = \left(\frac{W^2/2R}{\delta}\right)^2 \quad ; \quad \epsilon^{-1} = \left(\frac{W^2/2R}{t}\right)^2. \qquad [3]$$

When $\delta \gtrsim W^2/R$ (i.e., $\chi^{-1} \lesssim 1$), the wide gap requires no deflection, and the sheet remains flat (i.e., no confinement). If the gap is sufficiently small (i.e., $\chi^{-1} \gtrsim \epsilon^{-1}$), the stamp imposes perfect spherical shape, requiring a "bare" geometric strain $\varepsilon_{\rm bare} \sim (W/R)^2$, due to the elongation of its longitudes and shortening of latitudes. Our study focuses on the intermediate regime, $\epsilon^{-1} \gg \chi^{-1} \gg 1$, in which the sheet shape is strongly sensitive to confinement, but can relieve the energetically costly strain down to a residual value, $\varepsilon_{\rm res} \ll \varepsilon_{\rm bare}$, through deflections within the gap that are only penalized by their bending cost. We propose that these elastic deformations are described by a variant of Eq. **1**:

$$\text{Gauss-Euler } \textit{elastica}: \delta U_{\rm bend} = 0; \text{ subject to } U_{\rm strain}/U_{\rm bend} \to 0, \qquad [4]$$

where "$\to$" refers to the doubly asymptotic limit of high bendability and strong confinement, $\epsilon^{-1} \gg \chi^{-1} \gg 1$.

Eq. **4** describes an energy-minimization problem that is dominated by bending, while being constrained by the high cost of strain, much like the original *elastica* problem, but with two key and nontrivial distinctions. First, the minimization principle, $\delta U_{\rm bend} = 0$, means that, despite the presence of Gaussian curvature, the elastic energy is dominated by bending rather than strain; thus, Eq. **4** is closer to Euler's *elastica* (1) than to the generic FvK problem (2). Second, the suppression of strain that is expressed as an exact isometry constraint ($U_{\rm strain} = 0$) in Euler's *elastica* is now imposed in a weaker, asymptotic manner ($U_{\rm strain}/U_{\rm bend} \to 0$). Again, this latter distinction derives from the unavoidable distortion of a confined solid from its intrinsic metric due to a confining topography with $G_{\rm sub} \neq G_{\rm tar}$. We will show that the ratio $U_{\rm strain}/U_{\rm bend}$, and the deformed shape of the confined solid, are controlled by the confinement strength and bendability parameters, χ^{-1} and ϵ^{-1}, yielding distinct types of energy minimizers at various sectors of the parameter regime, $\epsilon^{-1} \gg \chi^{-1} \gg 1$.

We commence with a simpler model of a 2D sheet attached to a ball of stiff, radial springs (8–10). The relative simplicity of this "minimal" GIC problem enables a pedagogic exposition and an explicit derivation of the principle (4), which we then use to study spherical stamping.

Spherical Winkler Foundation

Consider a circular solid sheet of thickness t and radius W, made of Hookean solid of Young's modulus E, with stretching and bending moduli, $Y = Et$ and $B \propto Yt^2$, respectively. The sheet is attached to a stiff spherical surface of radius R; deflections away from the substrate are penalized by N radial, uniformly spaced harmonic springs, each spring with constant $4\pi R^2 K_{\rm sub}/N$ (Fig. 1 *G* and *H*). The energy density (per area), u, of the system is written schematically as:

$$u = u_{\rm strain} + u_{\rm bend} + u_{\rm sub}\ , \qquad [5]$$

where $u_{\rm strain} \sim Y \cdot (\text{strain})^2$, $u_{\rm bend} \sim B \cdot (\text{curvature})^2$, and $u_{\rm sub} \sim K_{\rm sub} \cdot (\text{deflection})^2$. The strain and curvature tensors, ε_{ij} and κ_{ij}, respectively, are given in terms of the in-plane displacements, u_r, u_θ, and normal deflection ζ of the sheet from its rest, planar state (*SI Appendix*). Here, the two dimensionless groups that quantify the strength of confinement and bendability of the sheet are defined as (8, 9):

$$\chi^{-1} = \frac{K_{\rm sub} R^2}{Y} \quad ; \quad \epsilon^{-1} = \frac{YW^4}{BR^2} \sim \left(\frac{W^2}{tR}\right)^2. \qquad [6]$$

The physical meaning of these parameters can be grasped by considering an ideal, axisymmetric deformation of the system. If $K_{\rm sub}$ is very small, the sheet remains nearly planar, and the energetic cost of flattening the substrate beneath it is $u_{\rm sub} \sim K_{\rm sub}(\frac{W^2}{R})^2$, whereas if $K_{\rm sub}$ is large, the substrate is barely deformed, and the sheet conforms to its spherical shape with characteristic energies, $u_{\rm bend} \sim B/R^2$ and $u_{\rm strain} \sim Y\varepsilon_{\rm bare}^2$ [where $\varepsilon_{\rm bare} \sim (W/R)^2$]. In this light, the dimensionless parameters in Eq. **6** are seen as the ratios $\chi^{-1} \sim \frac{u_{\rm sub}}{u_{\rm strain}}$, $\epsilon^{-1} \sim \frac{u_{\rm strain}}{u_{\rm bend}}$. Here, we focus on the regime:

$$\epsilon^{-1} \gg \chi^{-1} \gg 1 \quad \Longrightarrow \chi \ll 1\ ,\ (\epsilon/\chi) \ll 1\ , \qquad [7]$$

in which $K_{\rm sub}$ is large, and the substrate closely retains its shape to avoid a high-energy $u_{\rm sub}$. However, rather than conforming axisymmetrically to the substrate, which would generate a bare strain and an energy density, $u^{(\rm bare)} \approx u_{\rm strain} \sim Y\varepsilon_{\rm bare}^2$, the high bendability of the sheet enables a substantial suppression of strain, down to a residual level, $\varepsilon_{\rm res}$, via formation of small-wavelength wrinkles that "absorb" the excess length of compressed latitudes at the expense of only slight deviation of the substrate from its spherical shape.

The deformed shape and the residual strain can be found via a numerical simulation of the Seung–Nelson model of a 2D elastic sheet bound to a spherical Winkler foundation (11, 12), whose discrete elements capture the full geometrical nonlinearity underlying the FvK energy (*SI Appendix*). In our simulations (Fig. 2), we explore the relevant parameter regime (7) by fixing the confinement strength at a large value, $\chi^{-1} \simeq 39, 78, 156$ or 340, and gradually increasing the bendability, ϵ^{-1} (from 2×10^5 to 10^8), by reducing the sheet's thickness. As ϵ^{-1} exceeds a critical value (dashed vertical in Fig. 2 *G* and *H*), radial wrinkles emerge in an annular zone, $L<r<W$. Increasing ϵ^{-1} further, the wrinkles cover a larger and larger portion of the sheet, and their characteristic wavelength, λ, becomes smaller (Fig. 2*G*). We find that:

$$\lambda/W \approx 2\pi(\chi\epsilon)^{1/4} \;\;;\;\; L/W \simeq 2^{4/3}(\epsilon/\chi)^{1/6}. \qquad \textbf{[8]}$$

Analyzing the radial and hoop components of the in-plane stress tensor, $\sigma_{rr}(r), \sigma_{\theta\theta}(r)$ (which are linear combinations of the respective components of the strain tensor; *SI Appendix*), we find that, unlike the axisymmetric case, for which $\sigma_{rr}^{(\rm bare)} \sim \sigma_{\theta\theta}^{(\rm bare)} \sim Y\varepsilon_{\rm bare}$, here:

$$\sigma_{rr} \sim \sigma_{\theta\theta} \sim Y\cdot\varepsilon_{\rm res} \;\;, \text{where: } \varepsilon_{\rm res} \approx \sqrt{BK_{\rm sub}}/Y \;, \qquad \textbf{[9]}$$

(Fig. 2 *D–F*), such that $\varepsilon_{\rm res}/\varepsilon_{\rm bare} \sim \sqrt{\epsilon/\chi} \to 0$ in the limit (7). Let us recall that uniaxial compression of supported sheets yields wrinkles with wavelength λ of the form (8), reflecting suppression of compressive stress (here, $\sigma_{\theta\theta}$) down to residual level $\sim -\sqrt{BK_{\rm sub}}$ (obtained by balancing sheet bending and substrate stiffness) (13, 14). Fig. 2 *D–F* shows that not only the compressive hoop stress, $\sigma_{\theta\theta}$, but also the purely tensile radial stress, σ_{rr}, scales as $\sqrt{BK_{\rm sub}}$.

Further analysis of simulations reveals that the wrinkle-assisted suppression of stress (9) reshuffles the energetic hierarchy in the asymptotic limit (7). Fig. 2*H* shows that the strain energy is dominant at the vicinity of the threshold, but becomes negligible in comparison with the bending and substrate energies in the limit (7). This reversal of the energetic hierarchy can be understood through estimates of respective energy densities, which, at first pass, neglect spatial variation. Since Eq. **9** shows that all components of strain scale as $\varepsilon_{\rm res}$, we have that $u_{\rm strain} \sim Y\varepsilon_{\rm res}^2$, while $u_{\rm bend} \sim B(f/\lambda^2)^2$, where f is the characteristic amplitude of wrinkles; the wavelength, λ, is given by Eq. **8**; and $u_{\rm sub} \sim K_{\rm sub}f^2$. To estimate f, we use a "slaving" condition that links the wrinkle amplitude and wavelength, $(f/\lambda)^2 \sim (W/R)^2$, expressing the fact that the excess arclength "wasted" by azimuthal wrinkles matches the inward radial displacement of latitudes on the substrate (9, 10). We thus obtain:

$$u_{\rm bend} \sim u_{\rm sub} \sim u^{(\rm bare)}\sqrt{\epsilon/\chi} \;\;;\;\; u_{\rm strain}/u_{\rm bend} \sim \sqrt{\epsilon/\chi}\,. \qquad \textbf{[10]}$$

This result exhibits two critical features. First, the elastic energy is asymptotically vanishing in comparison with the bare energy, $u^{(\rm bare)} \sim Y\varepsilon_{\rm bare}^2$, required for perfectly conforming the flat sheet to a sphere. Second, the energetic hierarchy is reversed in comparison with the bare deformation—being governed by bending (and substrate deformation) rather than strain. Taken together, these two features manifest the Gauss–Euler principle (4). Notwithstanding the fact that imposing Gaussian curvature generates some strain in the sheet, its energetic cost is negligible, and the energy-minimizing state is found by minimizing bending energy (for this case, in balance with the substrate) over a family of "asymptotically isometric" configurations, in an analogous manner to Euler's *elastica* (1).

Inverted Tension Field Theory

Motivated by the numerical results, and by classical tension field theory (TFT), which describes an asymptotic, compression-free stress field in confinement problems that are governed by tensile boundary loads (3), we introduce here an "inverted" TFT (ITFT) that describes an asymptotic, strain-free stress field, in confinement problems governed by geometrical incompatibility. For the spherical Winkler problem, this theory is formulated as a doubly asymptotic expansion of FvK equations in χ and ϵ, around the

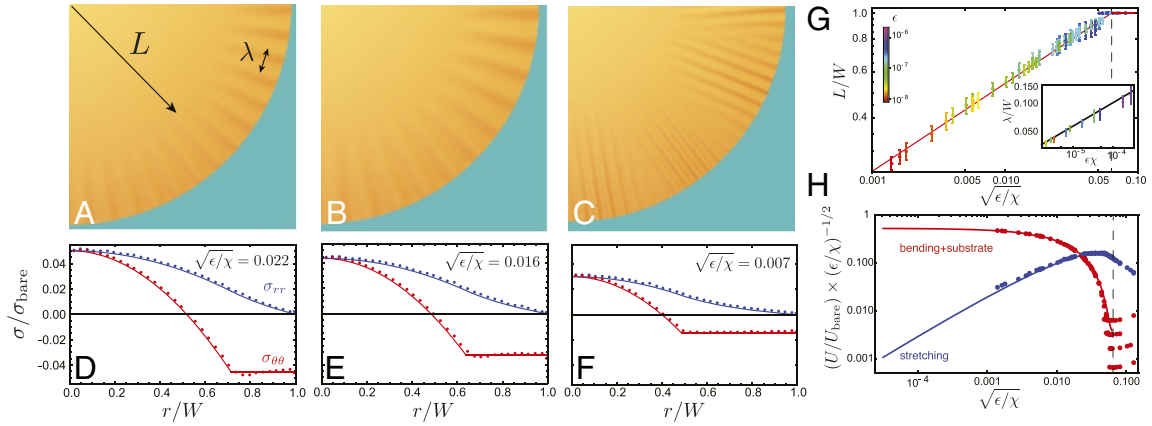

Fig. 2. (*A–C*) Top views of simulated circular sheets (gold) bound to spherical Winkler substrate (blue), with corresponding stress profiles of radial (σ_{rr}, blue) and hoop ($\sigma_{\theta\theta}$, red) components, shown in *D–F*. (*D–F*) Circles show stress computed from simulations and solid curves show ITFT predictions (*SI Appendix*). Stresses are normalized by the bare stress scale, $Y\varepsilon_{\rm bare} = Y(W/R)^2$. (*G*) Comparison of observed values of L (radius of unwrinkled core) and λ (wrinkle wavelength, measured at $r{=}W$; *Inset*), with ITFT predictions (Eq. **11** and *SI Appendix*) plotted as functions of ϵ/χ, the ratio of the inverse bendability (ϵ) and confinement strength (χ), Eq. **6**. Colors indicate the value of ϵ, and vertical dashed line denotes the wrinkling threshold. (*H*) Plots of the energy content in bending + substrate deformation (red) and strain energy (blue) for simulated sheets, showing that the ratio between strain and bending energies vanishes as $\epsilon/\chi \to 0$, as invoked by the Gauss–Euler *elastica* (Eq. **4**). Energies are normalized by the bare energy of the unwrinkled state ($\pi YW^6/(384R^4) \sim Y\varepsilon_{\rm bare}^2W^2$); ITFT predictions (*SI Appendix*) are shown in solid curves.

singular limit (7), to which we refer below by the symbol "$\rightarrow$". The succinct exposition below is supported by a detailed analysis of the displacement field, force balance equations, and energy balance in *SI Appendix*:

i. Hoop confinement: Elimination of radial strain—namely, preserving length of longitudes—requires a finite radial displacement: $\mathrm{u}_r(r) \rightarrow -\frac{1}{6}\frac{r^3}{R^2}$. This follows directly from the condition $\varepsilon_{rr} = \partial_r \mathrm{u}_r + \frac{1}{2}(\frac{\partial \zeta}{\partial r})^2 \rightarrow 0$, where $\zeta_{sph}(r) \approx -r^2/2R$. Consequently, the projection of the sheet's latitudes onto the sphere is contracted by: $\tilde{\Delta}(r) \equiv -\mathrm{u}_r/r \rightarrow \frac{1}{6}(\frac{r}{R})^2$.

ii. Wrinkle wavelength and hoop stress: Considering each latitude as an elastic hoop attached to a substrate of stiffness K_{sub} under confinement $\tilde{\Delta}(r)$, wrinkles relax the bare compressive strain, $\tilde{\Delta}(r)$—namely, $\zeta(r,\theta) \rightarrow \zeta_{sph}(r) + f(r)\cos(r\theta/\lambda)$—such that the amplitude, f, and wavelength, λ, satisfy the aforementioned slaving condition $(\frac{\pi f}{\lambda})^2 \rightarrow \tilde{\Delta}(r)$ (15). Minimizing bending and substrate energies, one obtains:

$$\lambda \approx 2\pi (B/K_{\mathrm{sub}})^{1/4} = W(\epsilon\chi)^{1/4}\ ;\ \sigma_{\theta\theta} \approx -2B/\lambda^2\ . \qquad [11]$$

iii. Radial stress: Turning now to force balance in the radial direction, we address the 2^{nd} FvK equation:

$$\partial_r(r\sigma_{rr}) - \sigma_{\theta\theta} = 0 \qquad [12]$$

$$\Longrightarrow \sigma_{rr} \rightarrow 2\sqrt{BK_{\mathrm{sub}}}(-1 + W/r)\ , \qquad [13]$$

where we used $\sigma_{\theta\theta}$ from Eq. **11** as a nonhomogeneous source for σ_{rr} along with the free boundary condition, $\sigma_{rr}|_{r=W} = 0$. Notably, Eq. **13** manifests the counterintuitive concept of "bending-induced" tension along wrinkles, which was envisioned already by Hure et al. (6).

iv. Strained core: The spatial divergence of radial stress, $\sigma_{rr} \sim r^{-1}$ in Eq. **13**, must be alleviated by a strained, unwrinkled core, $0<r<L$, whose radius vanishes asymptotically as $\chi, \epsilon \rightarrow 0$. The characteristic strain in this core is $(L/R)^2$, yielding a radial (and similarly, hoop) tension, $\sigma_{rr} \sim Y(L/R)^2$. The continuity of σ_{rr} at $r = L$ is required by radial force balance and yields the scaling relation, $L/W \sim (\epsilon/\chi)^{1/6}$, in accord with our simulations (8). Notably, the core-assisted regularization of radial stress (13) modifies our estimate of the strain energy (10) by only a logarithmic factor, $\log(W/L) \sim \log(\epsilon/\chi)$.

v. Vanishing shear: The above arguments explain why the radial and hoop stresses vanish as $\chi, \epsilon \rightarrow 0$. However, an asymptotically isometric configuration requires also the vanishing of shear stress, $\sigma_{r\theta} \rightarrow 0$, which is accommodated by way of small oscillations of radial displacement in registry with wrinkles, $\mathrm{u}_r \approx -r\tilde{\Delta} + (fr/R)\cos(r\theta/\lambda)$ (16). The energetic cost of these "shear cancelling" radial oscillations leads to curvature-induced stiffness, $K_{\mathrm{curv}} = Y/R^2$, that suppresses further the wrinkle amplitude. Taken together with the substrate stiffness, this leads to a generalized version of Eq. **11**:

$$\lambda = 2\pi (B/K_{\mathrm{eff}})^{1/4}\ ;\ K_{\mathrm{eff}} = K_{\mathrm{sub}} + K_{\mathrm{curv}}\ . \qquad [14]$$

(Since $\sigma_{rr} \ll K_{\mathrm{sub}} W^2$, another contribution to K_{eff}, due to tension along wrinkles (16), is negligible here.) Since $K_{\mathrm{curv}}/K_{\mathrm{sub}} = \chi \ll 1$, curvature-induced stiffness is also negligible here. However, we will show below that the elastic cost of shear suppression is critical for other GIC problems.

The solution of our ITFT equations yields quantitative expressions for the wavelength (Fig. 2*G*) and residual stresses (solid curves in Fig. 2 *D–F*), as well as the energies, U_{bend}, U_{sub}, and U_{strain} (Fig. 2*H*), in excellent agreement with simulations. This substantiates the Gauss–Euler *elastica* (4) and the ITFT equations, whose polar representation is Eqs. **11**, **12**, and **14**, as valuable tools for solving GIC problems.

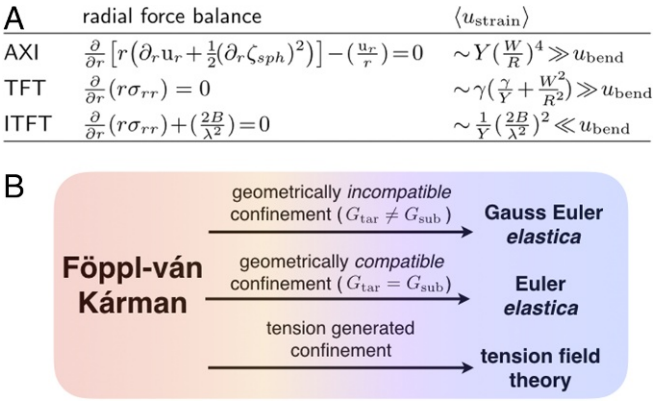

Fig. 3. (*A*) Three incarnations of radial force balance (12) for a spherically confined sheet, where $\langle u_{\mathrm{strain}} \rangle = U_{\mathrm{strain}}/\pi W^2$. Standard TFT addresses a tensile load γ at the edge, $r = W$, whose work is included in $\langle u_{\mathrm{strain}} \rangle$ [a logarithmic factor, $\log(W/L)$, is neglected from the energies of TFT and ITFT]. For simplicity, the axisymmetric equation is written for zero Poisson ratio. AXI, axisymmetric. (*B*) The mechanical equilibrium of a thin elastic solid is described by the FvK energy (2) and requires simultaneous minimization of straining and bending energies. As the bendability of the confined solid increases (arrows direction), the problem is described by an effective rule, depending on the conditions that generate confinement.

ITFT vs. TFT

We elucidate how ITFT embodies the Gauss–Euler *elastica* (4) by comparing the radial force balance equation and radial stress, Eqs. **12** and **13**, with their counterparts in two standard studies of a sheet attached to a spherical substrate (Fig. 3*A*).

The bare, axisymmetric (unwrinkled) state results from solving Eq. **12** by expressing the stress tensor through the axisymmetric displacement field (Fig. 3*A*, *Top*) (8), yielding a 2^{nd}-order equation for $\mathrm{u}_r(r)$. The consequent mean strain energy is $\langle u_{\mathrm{strain}} \rangle = U_{\mathrm{strain}}/\pi W^2 \sim Y\varepsilon_{\mathrm{bare}}^2$.

A TFT analysis of this problem (Fig. 3*A*) (8, 9) is suitable when a tensile load, $\gamma = \sigma_{rr}|_{r=W}$, is sufficiently smaller than $Y\varepsilon_{\mathrm{bare}}$, yet much larger than the residual hoop compression in a wrinkled state, $|\sigma_{\theta\theta}| \sim 2\sqrt{K_{\mathrm{sub}}B}$ (10). Under such conditions, Eq. **12** becomes a 1^{st}-order homogenous equation for the radial stress, and the asymptotic stress tensor has a single nonvanishing component: $\sigma_{ij} \rightarrow \gamma \begin{pmatrix} W/r & 0 \\ 0 & 0 \end{pmatrix}$, which underlies the dominant part of the energy.

In contrast, the ITFT stress yields a subdominant energy ($u_{\mathrm{strain}} \ll u_{\mathrm{bend}}$). Eq. **12** becomes an inhomogeneous equation for σ_{rr}, whose source ($\sigma_{\theta\theta}$) is set a priori by minimization of the bending energy, disregarding the explicit contribution of u_{strain} to the total energy. The asymptotic stress field has the form $\sigma_{ij} \rightarrow 2\sqrt{K_{\mathrm{sub}}B} \begin{pmatrix} -1 + W/r & 0 \\ 0 & -1 \end{pmatrix}$, acting as a tensorial Lagrange multiplier that generalizes the scalar Lagrange multiplier of Euler *elastica*.

The Spherical Stamping Problem

Spherical stamping differs from the Winkler-foundation problem in that there is no energetic penalty for deforming the spherical substrate. Instead, the energy consists only of bending and straining the sheet, subjected to the constraint that its deflection from the sphere is bounded: $|\zeta(r,\theta) - \zeta_{sph}(r)| \leq \delta$. A

qualitative understanding of this problem can be obtained by assuming that wrinkles fill the gap, such that the slaving condition, $(\pi f/\lambda)^2 = \tilde{\Delta}(r) \sim (r/R)^2$, implies a wrinkle wavelength $\lambda \sim \delta$ (up to r-dependent prefactors). The "local λ law" (Eq. **11**) then suggests that the gap effect is akin to a spherical Winkler substrate: $K_{\rm sub}(r) \sim B/\delta^4$ (*SI Appendix*) (16). The ITFT Eqs. **11** and **12** thus yield $|\sigma_{\theta\theta}| \sim \sigma_{rr} \sim B/\delta^2$. Using the results of the preceding analysis and recalling the dimensionless groups defined in Eq. **3**, we readily find that for a given ratio $\epsilon/\chi = (\delta/t)^2$, radial wrinkles cover the sheet barring a core of radius $L/W \sim (t/\delta)^{2/3}$. Evaluating the hoop and radial stresses and the various energies, one finds that: $U_{\rm bend}/U_{\rm bare} \sim (t/\delta)^2$ and $U_{\rm strain}/U_{\rm bend} \sim (t/\delta)^2$. Hence, the deformation satisfies the Gauss–Euler *elastica* (4) in the doubly asymptotic limit, $\chi, \epsilon/\chi \to 0$.

Note that if $\delta \gtrsim \sqrt{Rt}$ ($\chi \ll \epsilon^{1/2} \ll 1$), the gap-induced stiffness, $K_{\rm sub} = B/\delta^4$, falls below $K_{\rm curv} = Y/R^2$. In this regime, Eq. **14** restricts the wavelength to: $\lambda \sim \sqrt{Rt}$; consequently, wrinkles do not fill the gap (i.e., $f < \delta$). This reflects the energetic cost of suppressing shear strain when wrinkling about a curved shape; wrinkles with amplitude larger than $\sim\sqrt{Rt}$ would not satisfy $u_{\rm strain} \ll u_{\rm bend}$ and, thus, do not constitute an asymptotic solution of the Gauss–Euler *elastica* (4).

To obtain the actual ITFT solution for the spherical stamping problem, one has to consider a "three-zone" pattern: a "gap-limited" zone ($L_1 < r < W$), where the amplitude $f(r) = \delta$, maximizing deflection at the vicinity of the edge where confinement is strong; a "curvature-limited" zone ($L_2 < r < L_1$)—where the wavelength $\lambda \approx \sqrt{Rt}$ and $0 < f(r) < \delta$, so that wrinkles do not fill the gap; and, finally, a strained, unwrinkled core at $r < L_2$ (the geometry and distribution of stamp forces are described in *SI Appendix*). A central result of this analysis is the emergence of two "subphases" of ITFT (Fig. 4*B*): For $\epsilon \lesssim \chi < \epsilon^{7/10}$ ($t \lesssim \delta \lesssim t^{7/10}$), the pattern comprises only a gap-limited zone, which terminates sharply at an unwrinkled core [$L_1 = L_2 \sim W(t/\delta)^{2/3}$ in the above notations]; the intervening, curvature-limited zone appears when $\chi \sim \epsilon^{7/10}$ ($\delta \sim t^{7/10}$) and expands [with $L_2 \sim W(t/\delta)^{2/3}$ and $L_1 \sim \delta(R/t)^{1/2}$] upon increasing the gap until it reaches the outer edge at $\chi \sim \epsilon^{1/2}$ ($\delta \sim t^{1/2}$), at which stage a wrinkled state loses contact with the confining shells. Fig. 4*A* presents the energy U of our ITFT solution (normalized by $U_{\rm bare} = \pi Y W^6/384R^4$) and the related stamping force $F = 2\partial U/\partial\delta$, as a function of δ/t, for some values of the inverse bendability, ϵ, exhibiting two noteworthy features. First, each plot terminates at a finite value, $(\delta/t)_{max} \sim \epsilon^{-1/2}$, at which the wrinkle pattern is fully curvature-limited and detaches from the confining shells (signified by a vanishing stamping force). Second, as bendability increases, the energy relaxation becomes more efficient—the residual energy, $U_{\rm tot}$ at $(\delta/t)_{max}$ scales as $\epsilon^{1/2}\ U_{\rm bare}$.

Discussion

We introduced the Gauss–Euler *elastica* (4) for GIC problems—stating that bending is minimized subject to negligibility of strain energy. We demonstrated the applicability of this rule in two variants of a spherically confined sheet through ITFT—an asymptotic expansion of FvK equations around a singular, strain-free limit. We showed that the ITFT may be regarded an extension of Euler *elastica*, where the stress acts as a tensorial, spatially varying Lagrange multiplier that enforces asymptotic isometry. The schematic, Fig. 3*B*, shows how the highly nonlinear FvK problem for a confined sheet (2) recasts distinct simplifications as the sheet thickness becomes small: Euler *elastica* is applicable for developable deformations (no tension, no Gaussian curvature); TFT is applicable in the presence of tensile loads whose work dwarfs bending energy; and ITFT applies for GIC problems, where nondevelopable deformations emerge in the absence of tensile loads.

The GIC problem we addressed—confinement of a planar sheet onto a spherical topography—corresponds to $G_{\rm tar} < G_{\rm sub}$, where confinement is preferentially azimuthal, and the emerging wrinkle pattern is splayed. The GIC problem shown in Fig. 1*B* is characterized by $G_{\rm tar} > G_{\rm sub}$; there, confinement is preferentially radial, and wrinkles are bent. We expect that the Gauss–Euler *elastica* (4) is valid also for such problems, and even for more complex GIC problems that result in a mix of splay and bend of wrinkle textures (Fig. 1*D*).

Our analysis assumes that the minimal FvK energy (2) can be safely evaluated through the upper bound obtained by solving the ITFT equations for smooth, periodic deformations (*SI Appendix*). Notwithstanding the agreement between our simulations (Fig. 2) and solutions of the ITFT Eqs. **11**, **12**, and **14**, we emphasize that the validity of the rule (4) hinges on the validity of this central assumption, which awaits a rigorous mathematical proof. Furthermore, while our findings support the validity of Eq. **4** for the class of strong confinement problems addressed here, identified by finite, thickness-independent incompatibility,

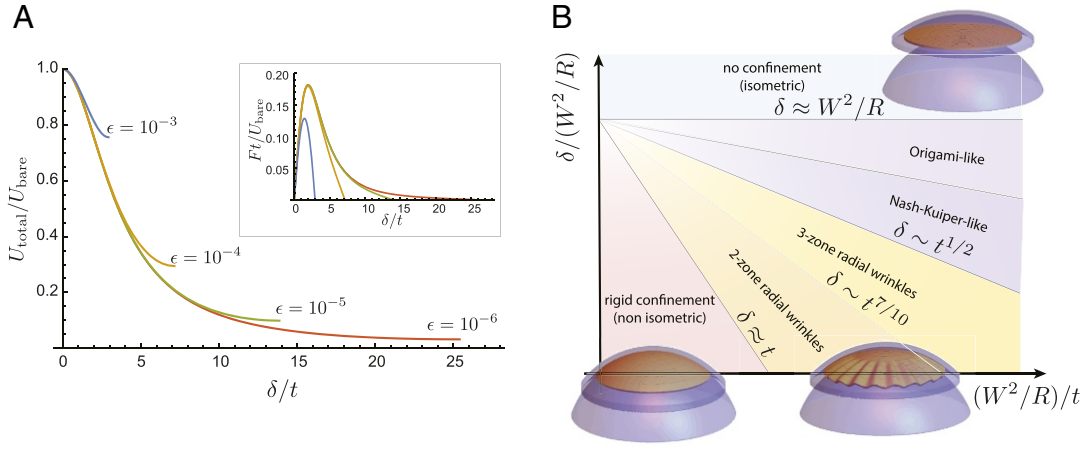

Fig. 4. ITFT predictions for the spherical stamping problem. (*A*) The predicted total energy, $U_{\rm tot}$, and force, $F = 2\partial_\delta U_{\rm tot}$ (*Inset*), plotted vs. the (normalized) gap separation δ/t, for a range of inverse bendability parameters. Energies are normalized by the bare energy (of axisymmetric state), $U_{\rm bare} = \pi Y W^6/(384R^4)$. Curves terminate at the point when wrinkles break contact with stamp, namely, $L_1 \to W$. (*B*) A schematic phase diagram of the spherical stamping problem, spanned by gap height δ and (inverse) sheet thickness t^{-1}, with the predicted regimes of two- or three-zone radial wrinkle patterns highlighted in orange/yellow.

$|G_{\rm tar} - G_{\rm sub}| \neq 0$, we suspect that it fails for a class of "weak confinement" problems for which the mismatch $|G_{\rm tar} - G_{\rm sub}|$ may eventually vanish with t. Well-known examples for this latter class of problems are the biaxial confinement of a stiff skin attached to a (planar) compliant substrate (13, 17, 18), and the contact of curved liquid surfaces with a planar sheet (19). The complexity of such problems can be anticipated by considering the two problems we addressed here in the parameter regimes complementary to Eq. **7**—namely, $\epsilon \ll 1, \chi/\epsilon \ll 1$. In the spherical Winkler problem, this corresponds to the regime, where the substrate is very soft and can deform substantially—flattening uniformly to reduce the sheet's strain and thereby developing stress-focusing, crumpled zones (19) or, alternatively, enabling the formation of localized folds (20–22).

For the spherical stamping problem, a parameter regime that corresponds to weak confinement is $\delta \gg \sqrt{Rt}$, where radial wrinkles predicted by ITFT no longer fill the gap, and another deformation is required to relax the residual energy, $\sqrt{t/\delta} \cdot U_{\rm bare}$, stored in a wrinkled state (Fig. 4*A*). To wit, let us consider a very weak confinement—namely, $\delta \sim t^\beta$, where $0 < \beta \ll 1$ (light purple in Fig. 4*B*); here, the sheet barely touches the confining shells, and the problem seems qualitatively similar to confining a sheet in a ball whose radius is only slightly smaller than its own (23). There, the deformation is governed by a few "stretching ridges" that separate the sheet into stress-free facets (5). Such a deformation is distinguished from a wrinkled state in two intimately related aspects. First, the ridges, which dominate the energy, are characterized by a balance of bending and strain (5), thereby obeying the general FvK rule (2), but not the restrictive version invoked in the Gauss–Euler *elastica* (4). Second, in contrast to wrinkle patterns, where curvature oscillates throughout the sheet, a network of ridges localizes curvature in "boundary layers" (whose width vanishes as $t \to 0$) and, consequently, there is an asymptotic divergence of curvature and discontinuity of slope between the two sides of each ridge, similarly to origami constructions.

The plausibility of origami-like deformations under weak confinement suggests yet another possibility of a smoother, but nevertheless nonwrinkly, deformation: Curvature, rather than slope, is spatially nonuniform, such that only the curvature's derivative is localized in a network of ridges and diverges as $t \to 0$ (heavy purple in Fig. 4*B*). Such a nontrivial pattern is suggested by Nash embedding theorem (24), whose relevance for the deformations of solid sheets has very recently begun to be explored (25). Whether such Nash mappings do characterize an asymptotically isometric response of confined solids, and whether their regularized versions (for small, but finite δ and t) are subjected to the Gauss–Euler *elastica* (4), are fascinating questions that we hope will inspire future studies.

ACKNOWLEDGMENTS. We thank P. Bella, R. V. Kohn, and N. Menon for many discussions; B. Roman, J. Bico, and J. Hure for discussing their experiment and model (6); R. Sknepnek for assistance with numerical simulations; D. Vella, D. O'Kiely, J. Bico, and J. Paulsen for useful comments; and participants of the program "Geometry and Elasticity of 2D Soft Matter," Kavli Institute for Theoretical Physics Santa Barbara 2016. This work was funded by American Chemical Society Petroleum Research Fund Grant 54513-ND and NSF Award CBET-14-38425. Simulations were performed by using the UMass Cluster at the Massachusetts Green High Performance Computing Center.

1. Levien R (2008) *The Elastica: A Mathematical History* (Univ of California, Berkeley), Technical report UCB/EECS-2008-103.
2. Landau LD, Lifschitz EM (1986) *The Theory of Elasticity* (Pergamon, Oxford).
3. Mansfield EH (1989) *The Bending and Stretching of Plates* (Cambridge Univ Press, Cambridge, UK).
4. Cerda E, Mahadevan L (1998) Conical surfaces and crescent singularities in crumpled sheets. *Phys Rev Lett* 80:2358–2361.
5. Witten TA (2007) Stress focusing in elastic sheets. *Rev Mod Phys* 79:643–675.
6. Hure J, Roman B, Bico J (2012) Stamping and wrinkling of elastic plates. *Phys Rev Lett* 109:054302.
7. Aharoni H, et al. (2017) The smectic order of wrinkles. *Nat Commun* 8:15809.
8. Grason GM, Davidovitch B (2013) Universal collapse of stress and wrinkle-to-scar transition in spherically confined crystalline sheets. *Proc Natl Acad Sci USA* 110:12893–12898.
9. Hohlfeld E, Davidovitch B (2015) Sheet on a deformable sphere: Wrinkle patterns suppress curvature-induced delamination. *Phys Rev E* 91:012407.
10. Bella P, Kohn RV (2017) Wrinkling of a thin circular sheet bonded to a spherical substrate. *Philos Trans A Math Phys Eng Sci* 375:20160157.
11. Seung HS, Nelson DR (1988) Defects in flexible membranes with crystalline order. *Phys Rev A* 38:1005–1018.
12. Vernizzi G, Sknepnek R, de la Cruz MO (2011) Platonic and Archimedean geometries in multicomponent elastic membranes. *Proc Natl Acad Sci USA* 108:4292–4296.
13. Bowden N, Brittain S, Evans AG, Hutchinson JW, Whiteside GM (1998) Spontaneous formation of ordered structures in thin films of metals supported on an elastomeric polymer. *Nature* 393:146–149.
14. Cerda E, Mahadevan L (2003) Geometry and physics of wrinkling. *Phys Rev Lett* 90:074302.
15. Davidovitch B, Schroll RD, Vella D, Adda-Bedia M, Cerda E (2011) Prototypical model for tensional wrinkling in thin sheets. *Proc Natl Acad Sci USA* 108:18227–18232.
16. Paulsen JD, et al. (2016) Curvature-induced stiffness and the spatial variation of wavelength in wrinkled sheets. *Proc Natl Acad Sci USA* 113:1144–1149.
17. Audoly B, Boudaoud A (2008) Buckling of a stiff film bound to a compliant substrate—Part I: Formulation, linear stability of cylindrical patterns, secondary bifurcations. *J Mech Phys Solids* 56:2401–2421.
18. Kohn RV, Nguyen HM (2013) Analysis of a compressed thin film bonded to a compliant substrate: The energy scaling law. *J Nonlinear Sci* 23:343–362.
19. King H, Schroll RD, Davidovitch B, Menon N (2012) Elastic sheet on a liquid drop reveals wrinkling and crumpling as distinct symmetry-breaking instabilities. *Proc Natl Acad Sci USA* 109:9716–9720.
20. Pocivavsek L, et al. (2008) Stress and fold localization in thin elastic membranes. *Science* 320:912–916.
21. Diamant H, Witten TA (2011) Compression induced folding of a sheet: An integrable system. *Phys Rev Lett* 107:164302.
22. Paulsen JD, et al. (2017) Geometry-driven folding of a floating annular sheet. *Phys Rev Lett* 118:048004.
23. Aharoni H, Sharon E (2010) Direct observation of the temporal and spatial dynamics during crumpling. *Nat Mater* 109:054302.
24. Nash J (1954) C^1-isometric imbeddings. *Ann Math* 9:383–396.
25. Gemmer J, Sharon E, Shearman T, Venkataramani SC (2016) Isometric immersions, energy minimization and self-similar buckling in non-Euclidean elastic sheets. *Europhys Lett* 114:24003.